Title

Sultam-Based Hetero[5]helicene: Synthesis, Structure, and Crystallization-Induced Emission Enhancement.

Journal

ACS omega, 1(6)

ISSN

2470-1343

Authors

Virk, Tarunpreet Singh
Ilawe, Niranjan V
Zhang, Guoxian
et al.

Publication Date

2016-12-01

DOI

10.1021/acsomega.6b00335

Peer reviewed

ACS OMEGA

Article

http://pubs.acs.org/journal/acsodf

Sultam-Based Hetero[5]helicene: Synthesis, Structure, and Crystallization-Induced Emission Enhancement

Tarunpreet Singh Virk,[†] Niranjan V. Ilawe,[‡] Guoxian Zhang,[†] Craig P. Yu,[†] Bryan M. Wong,[‡] and Julian M. W. Chan*[,†]

[†]Department of Chemistry and Biomolecular Sciences, University of Ottawa, 10 Marie Curie Pvt, Ottawa, Ontario, Canada K1N 6N5

[‡]Department of Chemical & Environmental Engineering, and Materials Science & Engineering Program, University of California at Riverside, Riverside, California 92521, United States

Supporting Information

ABSTRACT: A deep-blue-emitting sultam-based hetero[5]-helicene was synthesized in four steps, and its crystal structure and physical properties were characterized. The helicene displays more than two-fold crystallization-induced emission enhancement as well as atypical blue-shifting of its solid-state emission relative to the solution phase. This rapid synthesis of an unusual sulfonamide-based helicene fluorophore is expected to generate new molecular design options that will help address the ongoing challenges associated with designing pure-blue emitters for organic optoelectronic and sensing applications.

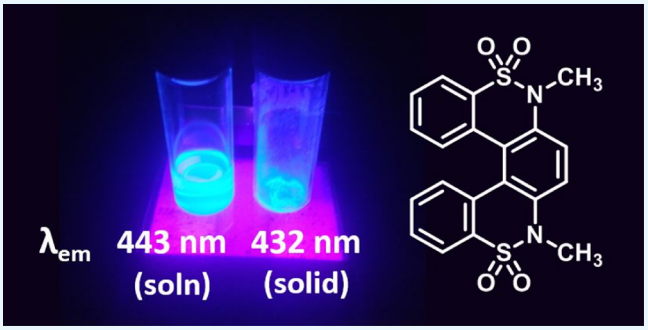

INTRODUCTION

Efficient luminescent organic materials show great promise for applications such as chemosensors, bioprobes, and solid-state lighting technology, for example, organic light-emitting devices (OLEDs).[1] Currently, there is much ongoing effort to develop organic materials that emit blue and deep-blue light, as opposed to sky-blue or blue-green. Compared with red and green organic luminogens, standard blue and deep-blue emitters are even more challenging to realize due to stability issues and the intrinsically wide bandgaps that are required.[2] To address this, recent research has sought to design new organic materials that are efficient and stable blue emitters.[3] Molecular design strategies have explored the use of anthracene,[4] fluorene,[5] polyphenylbenzene,[6] pyrene,[7] and carbazole-based[8] π-systems to generate the requisite large bandgaps for deep-blue emission. Regardless of the specific π-system, one issue that poses a constant challenge is that of aggregation-caused quenching (ACQ).[9] With most π-conjugated luminophores, aggregation due to $\pi-\pi$ stacking often results in red-shifted emissions[10] and a marked decrease in photoluminescence (PL) intensity.[11] Thus, a luminogen that is blue-emitting in solution might show undesirable blue-green emission and/or low PL efficiency in the solid state. This is a major problem for OLEDs, where organic emitters are employed as solid films. A possible solution lies in blue emitters that exhibit aggregation-induced emission (AIE) or crystallization-induced emission enhancement (CIEE) instead of ACQ. AIE, a property coined and studied extensively by Tang et al.,[12] describes luminogens that emit strongly as aggregates due to restricted intramolecular rotations (RIRs). CIEE,[13] a related but less common phenomenon, also avoids ACQ and allows a luminogen to emit more strongly in the solid than in solution. A subset of AIE is aggregation-induced blue-shifted emission (AIBSE), an intriguing property seen in some organic systems.[14] Compounds exhibiting AIBSE not only remain emissive in the solid phase, but also display blue-shifted instead of red-shifted emissions relative to solution. In this way, the desirable pure-blue emission is preserved. Although the underlying mechanism of AIBSE remains unclear, Shuai and co-workers propose that it stems from the smaller reorganization energies in aggregates versus solution phase, as a consequence of restricted geometric relaxation, excited-state planarization, and the freezing of low-frequency out-of-plane vibrations.[15] As research into the microscopic origin of AIBSE continues, better defined structure−property relationships will be established to guide the rational design of future organic "AIBSEgens". Considering the theoretical and technological implications, it is important to develop new AIE- and CIEE-active materials that retain high-intensity pure-blue emissions in the solid state. Herein, we report the four-step synthesis of a sulfonamide-based hetero[5]helicene **4** showing deep-blue emission in solution and solid phase, as well as CIEE- and AIBSE-like properties in the crystalline state.

RESULTS AND DISCUSSION

The structure of **4** is a polycyclic aromatic π-framework composed of three benzene rings and two sultam rings fused together (Figure 1). As is the case with [n]helicenes,

Received: October 23, 2016
Accepted: December 9, 2016
Published: December 20, 2016

DOI: 10.1021/acsomega.6b00335
ACS Omega 2016, 1, 1336−1342

Figure 1. Structure of blue-emitting hetero[5]helicene **4**.

intramolecular steric repulsion gives rise to a torsion angle that reduces conjugation and widens the bandgap. Using DFT calculations at the M06-2X/6-311G(d,p) level of theory, we calculated the racemization barrier of **4** to be 20.08 kcal/mol at 298 K. With helicene **4**, the incorporation of two sulfonamide moieties into the rigid framework was expected to further increase the torsion angle by virtue of the larger third-row element (sulfur) and the nitrogen atom with partial sp^3 character. The S–N bridges, which possess double bond character,[16] also serve to rigidify the system and further restrict intramolecular rotations. Although they have been ubiquitous in medicinal chemistry for decades, sulfonamide functional groups in the context of organic optoelectronic materials are still extremely rare.

To prepare helicene **4**, we began the synthesis (Scheme 1) with the cheaply available phenylene-1,4-diamine. The diamine was refluxed with two equivalents of 2-nitrobenzenesulfonyl chloride in the presence of pyridine for 2 h to generate bis-sulfonamide **1** in 82% isolated yield. In the second step, the nitro groups were reduced with stannous chloride to afford two aniline moieties that are poised for a double Pschorr cyclization. This key step was achieved by first diazotizing the pair of primary amines with isoamyl nitrite, followed by diradical generation via one-electron reduction with aqueous potassium ferrocyanide, and finally double-ring closure to give the unsubstituted hetero[5]helicene **3** as one of the major products. The double cyclization is not regioselective, in that the nonhelical hetero[5]phenacene is obtained as the other main product when the second cyclization occurs para instead of ortho to the first newly formed C–C bond. Owing to its less planar structure, hetero[5]helicene **3** was significantly more soluble in organic solvents than the hetero[5]phenacene regioisomer, thus allowing for facile separation. Complete purification of **3** was achieved using standard silica gel column chromatography. In the last step, **3** underwent double N-methylation to yield **4**. The higher acidity of the sulfonamide NH compared to that of amides allows for facile N-functionalization under more mildly basic conditions. Hence, the unsubstituted helicene **3** can serve as a readily accessible precursor to a wide range of functional hetero[5]helicenes, where different side chain modifiers can be introduced by N-functionalization, thus allowing for the facile fine tuning of materials properties. Upon obtaining *N,N′*-dimethyl hetero[5]-helicene **4**, its molecular structure was unambiguously confirmed by ^1H and ^{13}C NMR, electrospray ionization mass spectrometry (ESI-MS), and single-crystal X-ray diffraction studies. To assess the thermal stability of hetero[5]helicene **4**, we carried out thermogravimetric analysis (TGA) of the solid under nitrogen (Figure S12). Compound **4** was found to be

Scheme 1. Synthesis of Sultam-Based Hetero[5]helicene 4

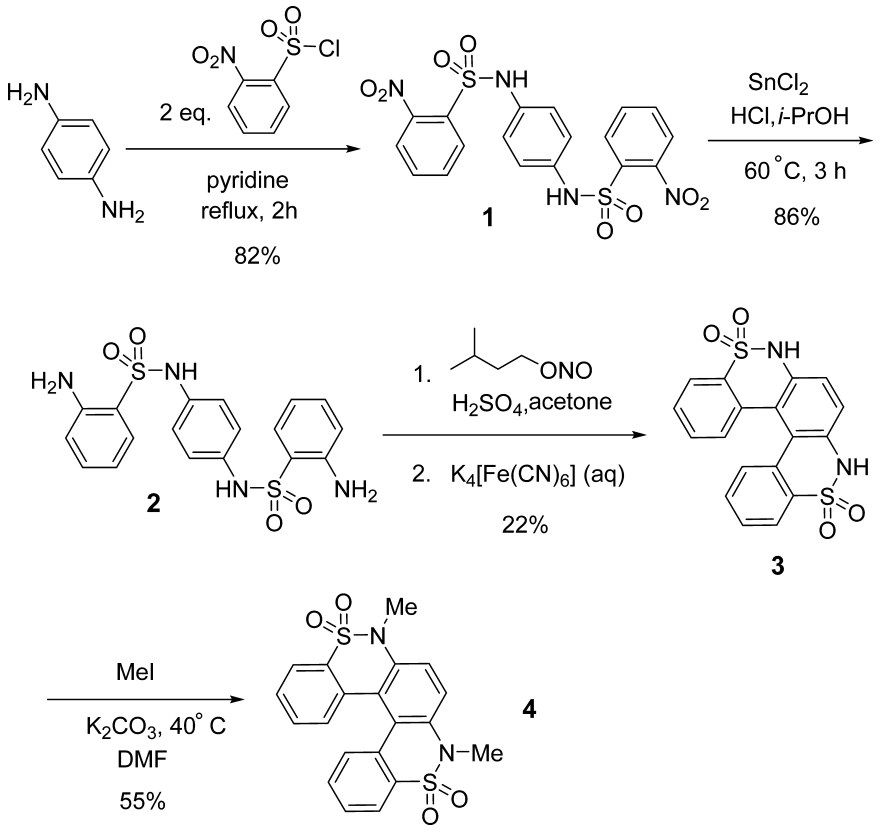

DOI: 10.1021/acsomega.6b00335
ACS Omega 2016, 1, 1336–1342

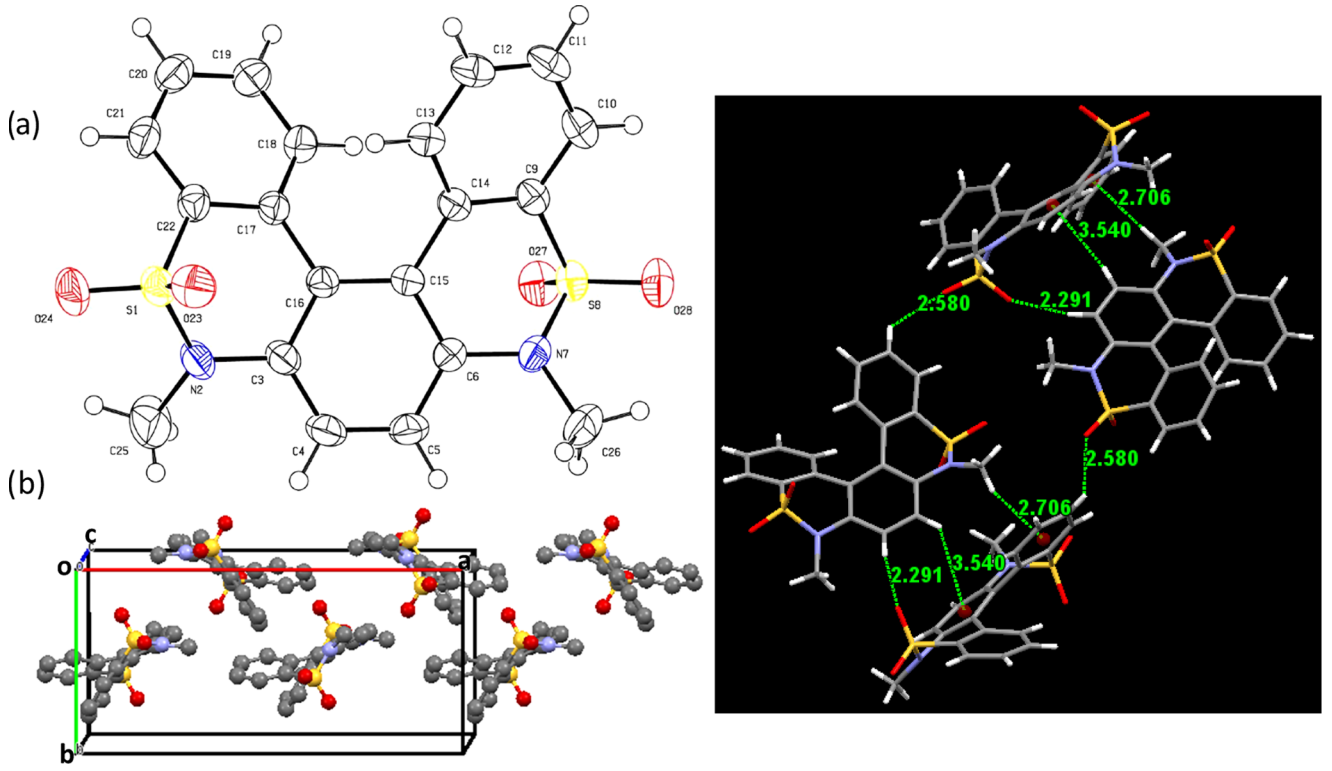

Figure 2. Single-crystal X-ray studies: (a) ORTEP structure of **4**, (b) crystal-packing diagram viewed along the crystallographic *c*-axis showing a herringbone-like arrangement of helicene molecules (hydrogens omitted for clarity), (c) expanded view of the crystal-packing structure showing short-range intermolecular C−H···π and hydrogen-bonding interactions.

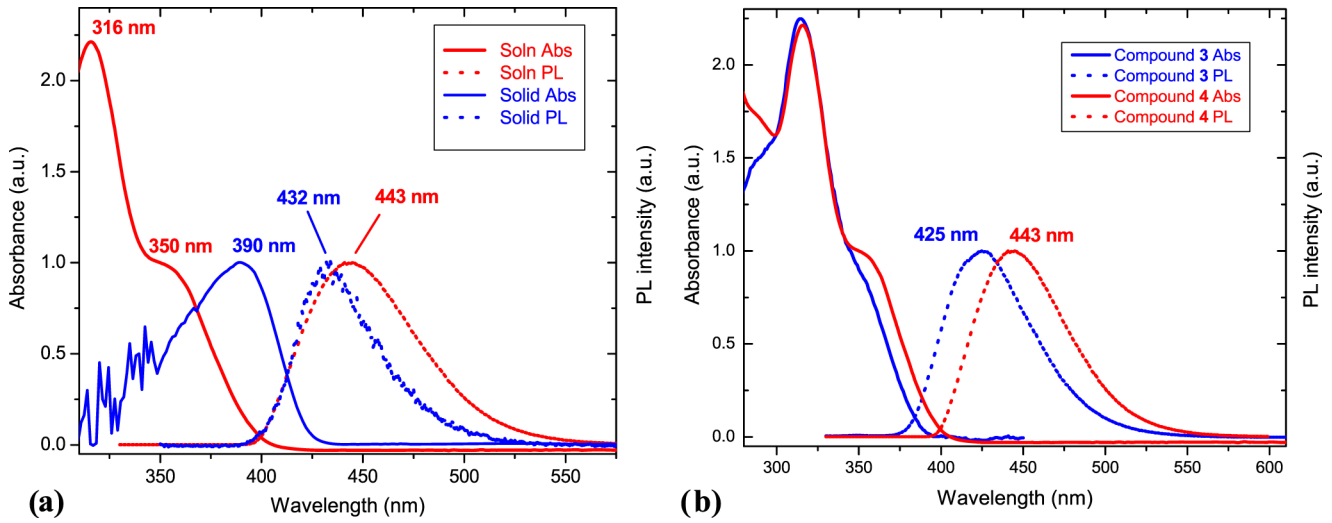

Figure 3. (a) Solution (DCM) and solid-state UV−vis absorbance and PL spectra of hetero[5]helicene **4**. (b) Comparison of the solution UV−vis absorption and PL of the hetero[5]helicenes **3** (unsubstituted) and **4** (dimethylated).

thermally robust with its high thermal decomposition temperature of 300.8 °C (i.e., T_d, corresponding to 5% weight loss). Good thermal stability is important for optoelectronic applications, as the material must withstand the resistive heating that occurs in organic electronic devices (e.g., OLEDs),[17] as well as the temperatures used in the vacuum sublimation stage of device fabrication.

From the single-crystal structure, racemic hetero[5]helicene **4** is observed to form orthorhombic crystals of the space group *Pbca* with a = 18.9965(18) Å, b = 8.9214(9) Å, c = 22.156(2) Å, $\alpha = \beta = \gamma = 90°$. The molecules are seen to pack in a herringbone-type arrangement with no significant $\pi-\pi$ stacking interactions (Figure 2b). The intermolecular edge-to-face distance was measured to be 3.540 Å, and the herringbone slip angle was found to be 47.44°. The lack of face-to-face $\pi-\pi$ stacking was expected, given the nonplanar nature of the hetero[5]helicene. Indeed, the single-crystal structure revealed a torsion angle of 20.8°, which precludes efficient π-stacking and incidentally widens the electronic bandgap. This is significant because eliminating strong $\pi-\pi$ interactions in the solid state is key in preventing the formation of H-aggregates and excimers,[9] many of which show ACQ that result in

DOI: 10.1021/acsomega.6b00335
ACS Omega 2016, 1, 1336−1342

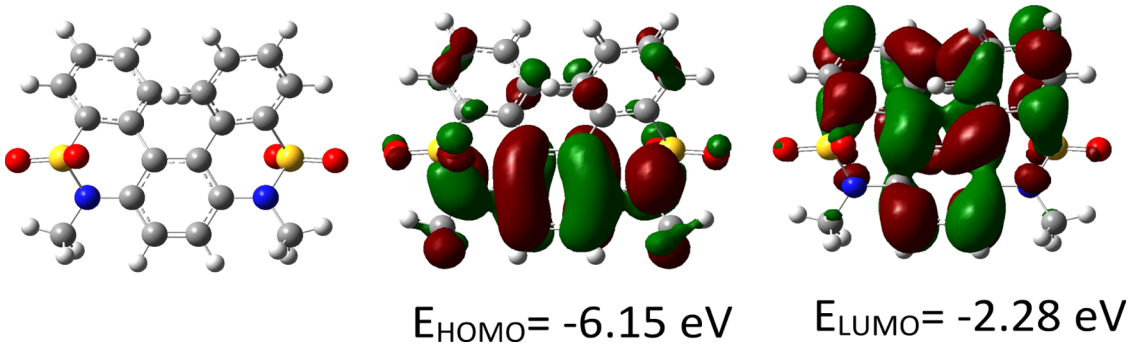

Figure 4. Optimized molecular structure of hetero[5]helicene **4** and its frontier molecular orbitals, calculated with Gaussian09 using the B3LYP/6-311G(d) method.

diminished or zero emission. The single-crystal structure also revealed numerous short intermolecular interactions, such as C−H···π and C−H···O hydrogen-bonding interactions (Figure 2c). Specifically, there exist several aromatic C−H···π interactions with atom-to-centroid distances measuring 3.540 Å, and shorter (2.706 Å) aliphatic C−H···π interactions between the methyl protons and outer benzene rings of the fused polycyclic π-system. In addition, short intermolecular C−H···O interactions between aromatic protons and sulfonamide oxygen atoms were also observed, with distances measuring 2.291 and 2.580 Å. The multitude of short-range interactions between the hetero[5]helicene molecules in the solid state likely helps in restricting intramolecular motion and rotations.

To characterize the photophysical properties of hetero[5]-helicene **4**, we carried out UV−vis and fluorescence studies in the solution phase and solid state. In dilute dichloromethane (DCM) solution, **4** showed major absorption peaks at 316 and 350 nm (shoulder), a deep-blue fluorescence emission band at 443 nm (Figure 3a), and a fluorescence lifetime of 1.565 ns. In comparison, the unsubstituted precursor, helicene **3**, showed violet emission with a peak at 425 nm (Figure 3b). In the solid state, peak absorption of **4** was observed at 390 nm, and notably, the fluorescence band appeared at 432 nm. This hypsochromic shift of the solid-state emission relative to the solution emission is characteristic of the unusual AIBSE phenomenon.

In their theoretical study,[15] Shuai and co-workers proposed an explanation for AIBSE using an adiabatic potential-energy surface model. The emission energy (E_{em}) is given as the difference between the absorption energy (E_{ab}) and the total reorganization energy (λ)

$$E_{em} = E_{ab} - \lambda \quad (1)$$

Going from the aggregated state (agg) to the solution (sol) phase, the shift in emission is thus simply given by

$$\Delta E_{em}^{agg\text{-}sol} = \Delta E_{ab}^{agg\text{-}sol} + \lambda^{sol\text{-}agg} \quad (2)$$

In conventional organic fluorophores where the aggregate emission is red-shifted with respect to the solution, the $\Delta E^{agg\text{-}sol}$ term is <0. As highlighted by Shuai's group, it is possible to obtain AIBSE (i.e., $\Delta E_{em}^{agg\text{-}sol} > 0$) in aggregates if the absorption shift going from solution to aggregate is relatively small while the $\lambda^{sol\text{-}agg}$ term (corresponding to the Stokes shift) in eq 2 is large. In our present system, this was indeed observed experimentally. In dilute solution, hetero[5]helicene **4** shows a large Stokes shift of almost 100 nm, whereas the corresponding value in the solid state is only about 40 nm. This gives rise to a large positive $\lambda^{sol\text{-}agg}$ term. At the same time, the difference between absorption peak values in solution (350 nm) versus solid state (390 nm) is not very large, that is, the $\Delta E_{ab}^{agg\text{-}sol}$ term is small. The net result is that the emission (443 nm) of the solution phase is blue-shifted (to 432 nm) in the solid. The absence of red-shift in the solid-state PL allows the deep-blue emission to be preserved. At the molecular level, this AIBSE behavior in **4** is likely due to the aforementioned lack of π-stacking and RIR in the solid state. Although there are no significant intermolecular π−π interactions within the crystalline phase of **4**, collectively there exist a multitude of intermolecular C−H···π and C−H···O interactions of short contact distances (Figure 2c) to help stabilize crystal packing and restrict intramolecular rotational motions, leading to blue-shifted and enhanced emission. By virtue of the rigid and fused nature of the hetero[5]helicene π-system, as well as the numerous short-range intermolecular interactions in the crystalline state, the blue-shifted emission most likely results from restricted geometric change and smaller reorganization energies[15] in the solid compared to the solution phase. In addition to blue-shifted emission, helicene **4** also displayed remarkable CIEE, in that the PL efficiency of the crystals was twice as high as the solution. The fluorescence quantum yield (Φ_f) of **4** in DCM was measured to be 13%, whereas single crystals and ground crystals had Φ_f values of 22 and 28%, respectively (cf. the solid-state PL efficiencies of the OLED polymers, PPV and MEH-PPV, are 27 and 15%,[18] respectively). With **4**, we attribute the higher PL efficiency of milled versus pristine crystals to the suppression of reabsorption effects, as described by Katoh et al.[19]

With regard to the optical bandgap of **4**, the highest occupied molecular orbital (HOMO)−lowest unoccupied molecular orbital (LUMO) gap was estimated from its UV−vis absorption edge using the Tauc method and was found to be approximately 3.1 eV, typical of a wide-bandgap semiconductor. In comparison, the theoretical HOMO−LUMO gap that we obtained through density functional theory (DFT) calculations using the B3LYP/6-311G(d) method was 3.87 eV. The HOMO and LUMO energy levels were calculated to be −6.15 and −2.28 eV, respectively, in vacuum (Figure 4), which agreed with the electrochemically determined values within 0.4 eV (see cyclic voltammetry data in the Supporting Information). We also performed calculations to ascertain the fluorescence emission energies (solventless) of dialkylated and diacylated derivatives of our sultam-based helicene core (see the Supporting Information). The N-alkylated derivatives were found to have fluorescence emission energies of 3.04 eV (407 nm) in vacuum (vs 414 nm in DCM), whereas the N-acylated

DOI: 10.1021/acsomega.6b00335
ACS Omega 2016, 1, 1336−1342

analogues showed higher calculated emission energies of 3.38 V (367 nm) in vacuum (vs 360 nm in DCM). These computational results suggest that it could be interesting to initiate future investigations into various acyl derivatives to determine whether the reported [5]helicene core is promising as a common platform for even wider bandgap materials that emit in the violet or near-UV regions. Efficient and stable blue-violet[20] and UV[21] organic emitters are also materials of current interest, and the ease with which the bandgap of our sultam-based core can be tuned, based on N-substituent choice, holds promise for further future investigations into the modular design and synthesis of novel blue-to-UV emitters.

CONCLUSIONS

In summary, we have designed and synthesized a novel sultam-based hetero[5]helicene with intriguing optoelectronic properties. Helicene **4** displays deep-blue emission in solution and in the solid state. Upon crystallization, the PL efficiency does not suffer from ACQ effects, but is instead enhanced two-fold. In addition to CIEE, the solid-state emission is also atypically blue-shifted relative to the solution emission, thus preserving the desirable deep-blue wavelength. TG studies also highlighted the excellent thermal stability of **4**, whereas DFT calculations showed that the bandgap of the hetero[5]helicene core could be easily tuned. We believe that these properties will make this sultam-based helicene motif a very promising paradigm for designing next-generation pure-blue emitters, especially considering the fact that sulfonamides remain highly underutilized in organic electronics.

EXPERIMENTAL SECTION

Materials and Methods. For the synthesis of compounds, all reactions requiring anhydrous conditions were carried out in oven-dried glassware under dry nitrogen using standard Schlenk techniques. All reagents and chemicals were purchased from Sigma-Aldrich or Fisher and used without further purification. Reaction solvents were dried over activated 3 Å molecular sieves. Crude products were purified by flash column chromatography on silica gel 60−230 mesh. ^{1}H and ^{13}C NMR spectra were recorded on a Bruker AVANCE II 400 MHz NMR spectrometer. ESI-MS spectra were recorded on a Micromass, Q-Tof-2 mass spectrometer. UV−vis spectra were recorded on a Scandrop MBI spectrophotometer, using a quartz cuvette (1 cm path length) and AR grade DCM as the solvent. PL spectra were recorded on a Photon Technology International (PTI) spectrofluorometer equipped with an LPS-220B lamp power supply (PTI) and a PTI 814-Detector system. Diffuse reflectance spectra (DRS) were obtained using a Varian Cary 100 UV−vis spectrophotometer, equipped with a diffuse reflectance accessory consisting of a 73-mm diameter integrating sphere. Solid-state fluorescence studies were performed using a PerkinElmer Luminescence Spectrometer LS 50 instrument, and solid-state quantum efficiencies were determined by the integrating sphere technique using a quanta-φ F-3029 sample chamber of the Horiba Scientific Fluorolog-3 spectrofluorometer equipped with an integrating sphere of diameter 15.2 cm coated with Spectralon material. TGA data were recorded on a Q5000 IR instrument (TA Instruments; New Castle, DE), and the sample was heated from 25 to 500 °C with a temperature rise of 10 °C/min under nitrogen flow (120 mL/min). TGA data were analyzed using TA Instruments Universal Analysis 2000 Version 4.5 A. Cyclic voltammetry (CV) studies were carried out on a PARSTAT 2273 electrochemical workstation with a conventional three-electrode configuration consisting of a platinum wire working electrode, a platinum mesh counter electrode, and a silver wire pseudo-reference electrode. The experiments were performed at room temperature using 5×10^{-4} M solutions of analyte in HPLC-grade acetonitrile with 0.1 M tetra-*n*-butylammonium hexafluorophosphate ($TBAPF_6$) as the supporting electrolyte. Deoxygenation of the solutions was achieved by sparging with nitrogen for 30 min, and the working electrode was cleaned after each run. The cyclic voltammograms were recorded using a scan rate of 100 mV s^{-1}. Potentials measured with reference to the Ag electrode were converted to values vs. the saturated calomel electrode (SCE) by means of a ferrocenium/ferrocene (F_c^+/F_c) internal standard.

***N,N′*-(1,4-Phenylene)bis(2-nitrobenzenesulfonamide) (1).** Bis-sulfonamide **1** was prepared under sulfonamide synthesis conditions described in the literature. Phenylene-1,4-diamine (2.00 g, 18.5 mmol) and 2-nitrobenzenesulfonyl chloride (8.20 g, 37.0 mmol) were added to pyridine (19 mL) in a flask, and the mixture was stirred under reflux at 110 °C for 2 h. The reaction mixture was then cooled to room temperature and treated with ice-cold water. The suspension was then filtered, and the precipitate thus obtained was washed successively with water, hot methanol, and diethyl ether to afford the product as a tan-colored solid (yield: 7.79 g, 88%); mp 261−263 °C. The product was analyzed by ^{1}H and ^{13}C NMR (see the Supporting Information for NMR spectra of all compounds), compared against literature values, and used directly in the next step.

***N,N′*-(1,4-Phenylene)bis(2-aminobenzenesulfonamide) (2).** To a suspension of compound **1** (5.00 g, 10.5 mmol) in 50 mL of isopropanol at 55 °C was added stannous chloride dihydrate (20.0 g, 88.6 mmol) in a portion-wise manner. Then, 36% hydrochloric acid (18 mL) was added dropwise using a dropping funnel over the course of 30 min. The entire mixture was then heated with stirring at 60 °C for 3 h. The reaction mixture was then cooled to room temperature and subsequently immersed in an ice bath. The resulting precipitates were filtered and then washed successively with water, methanol, and diethyl ether to yield the diamine as a tan-colored powder (yield: 3.81 g, 87%); mp 253−254 °C. The product was analyzed by ^{1}H and ^{13}C NMR, compared against published values, and used directly in the next step.

***N,N′*-Dihydro-2,7-dithia-3,6-diaza[5]helicene-*S,S,S′,S′*-tetraoxide (3).** Compound **2** (0.0500 g, 0.119 mmol) was dissolved in acetone (7 mL) and H_2SO_4 (0.026 mL, 0.48 mmol) was added dropwise at 0 °C followed by isoamyl nitrite (0.064 mL, 0.48 mmol). The mixture was stirred for 1 h, and then water was added until the solution became homogeneous. After 1 h, potassium ferrocyanide trihydrate (0.252 g, 0.598 mmol) dissolved in deionized water (18 mL) was added dropwise to the above reaction mixture. The reaction was then stirred for an additional 4 h, after which it was cooled in an ice bath and filtered. The precipitate was washed with cold water and then air-dried. The crude product was subsequently chromatographed on a silica gel column, to afford **3** as a white powder (yield: 0.010 g, 22%); mp 342−344 °C. ^{1}H NMR (400 MHz, MeOD): δ (ppm) 7.97−7.95 (d, 2H, J = 8 Hz), 7.59−7.55 (t, 2H, J = 8 Hz), 7.49−7.47 (d, 2H, J = 8 Hz), 7.42−7.38 (t, 2H, J = 8 Hz), 7.27 (s, 2H); ^{13}C NMR (100 MHz, DMSO-d_6): δ (ppm) 135.8, 134.8, 131.6, 131.3, 129.4,

DOI: 10.1021/acsomega.6b00335
ACS Omega 2016, 1, 1336−1342

122.7, 121.6, 121.4. ESI-MS: calcd 383.0160, found 383.0186 (M^-).

***N,N′*-Dimethyl-2,7-dithia-3,6-diaza[5]helicene-*S,S,S′,S′*-tetraoxide (4).** A mixture of **3** (0.050 g, 0.13 mmol), K_2CO_3 (0.054 g, 0.39 mmol, 3 equiv), and methyl iodide (0.028 mL, 0.455 mmol) in 0.80 mL of DMF was stirred at 40 °C for 12 h. At the end of the reaction, 3 mL of deionized water was added to the reaction vessel, and the mixture was acidified dropwise with 2 M HCl to a pH of 3−5, as indicated by pH paper. The aqueous mixture was extracted with DCM (3 × 30 mL), and the combined extracts were dried over anhydrous magnesium sulfate, filtered, and concentrated by rotary evaporation. The crude mixture was chromatographed on a silica gel column (3:7 v/v ethyl acetate in hexanes) to furnish dimethylated hetero[5]helicene **4** as a white solid (yield: 0.030 g, 55%); mp 297−299 °C. ^{1}H NMR (400 MHz, $CDCl_3$): δ (ppm) 7.98−7.96 (m, 2H), 7.53−7.49 (m, 2H), 7.45 (s, 2H), 7.41−7.39 (m, 2H), 7.34−7.30 (m, 2H), 3.38 (s, 6H); ^{13}C NMR (100 MHz, $CDCl_3$): δ (ppm) 138, 134.8, 132.8, 132.3, 131.1, 128.6, 124.4, 122.5, 121.9, 34.9. ESI-MS: calcd 435.0449, found 435.0489 (M + Na).

■ ASSOCIATED CONTENT

Supporting Information

The Supporting Information is available free of charge on the ACS Publications website at DOI: 10.1021/acsomega.6b00335.

^{1}H and ^{13}C NMR spectra, single-crystal structure data and Cartesian coordinates, Commission Internationale de l'Eclairage (CIE) color space chromaticity diagrams, fluorescence spectra from aggregation studies, and TGA curve (PDF)

■ AUTHOR INFORMATION

Corresponding Author

*E-mail: julian.chan@uottawa.ca.

ORCID

Bryan M. Wong: 0000-0002-3477-8043

Julian M. W. Chan: 0000-0002-2734-6496

Notes

The authors declare no competing financial interest.

■ ACKNOWLEDGMENTS

This work was financially supported by the Natural Sciences and Engineering Research Council (NSERC Discovery Grant; RGPIN-2016-04614), the CFI John R. Evans Leaders Fund (CFI-JELF Project No. 34474), the Ministry of Research and Innovation (MRI), and the University of Ottawa. B.M.W. and N.V.I. acknowledge the University of California, Riverside, for financial support, and the National Science Foundation for the use of supercomputing resources through the Extreme Science and Engineering Discovery Environment (XSEDE), Project No. TG-CHE150040.

■ REFERENCES

(1) (a) Chao, T. C.; Lin, Y. T.; Yang, C. Y.; Hung, T. S.; Chou, H. C.; Wu, C. C.; Wong, K. T. *Adv. Mater.* **2005**, *17*, 992−996. (b) Uoyama, H.; Goushi, K.; Shizu, K.; Nomura, H.; Adachi, C. *Nature* **2012**, *492*, 234−240. (c) Tang, C. W.; Vanslyke, S. A. *Appl. Phys. Lett.* **1987**, *51*, 913−915. (d) Grimsdale, A. C.; Chan, K. L.; Martin, R. E.; Jokisz, P. G.; Holmes, A. B. *Chem. Rev.* **2009**, *109*, 897−1091. (e) Kamtekar, K. T.; Monkman, A. P.; Bryce, M. R. *Adv. Mater.* **2010**, *22*, 572−582.

(2) (a) Farinola, G. M.; Ragni, R. *Chem. Soc. Rev.* **2011**, *40*, 3467−3482. (b) Gather, M. C.; Köhnen, A.; Meerholz, K. *Adv. Mater.* **2011**, *23*, 233−248.

(3) (a) Yang, X.; Xu, X.; Zhou, G. *J. Mater. Chem. C* **2015**, *3*, 913−944. (b) Hua, W.; Liu, Z.; Duan, L.; Dong, G.; Qiu, Y.; Zhang, B.; Cui, D.; Tao, X.; Cheng, N.; Liu, Y. *RSC Adv.* **2015**, *5*, 75−84. (c) Lee, J.; Chen, H.-F.; Batagoda, T.; Coburn, C.; Djurovich, P. I.; Thompson, M. E.; Forrest, S. R. *Nat. Mater.* **2016**, *15*, 92−98. (d) Huang, J.; Sun, N.; Chen, P.; Tang, R.; Li, Q.; Ma, D.; Li, Z. *Chem. Commun.* **2014**, *50*, 2136−2138. (e) Chercka, D.; Yoo, S.-J.; Baumgarten, M.; Kim, J.-J.; Müllen, K. *J. Mater. Chem. C* **2014**, *2*, 9083−9086. (f) Shi, L.; Liu, Z.; Dong, G.; Duan, L.; Qiu, Y.; Jia, J.; Guo, W.; Zhao, D.; Cui, D.; Tao, X. *Chem. Eur. J.* **2012**, *18*, 8092−8099.

(4) Zheng, C. J.; Zhao, W. M.; Wang, Z. Q.; Huang, D.; Ye, J.; Ou, X. M.; Zhang, X. H.; Lee, C. S.; Lee, S. T. *J. Mater. Chem.* **2010**, *20*, 1560−1566.

(5) Polo, F.; Rizzo, F.; Gutierrez, M. V.; Cola, L. D.; Quici, S. *J. Am. Chem. Soc.* **2012**, *134*, 15402−15409.

(6) Zhan, X.; Sun, N.; Wu, Z.; Tu, J.; Yuan, L.; Tang, X.; Xie, Y.; Peng, Q.; Dong, Y.; Li, Q.; Ma, D.; Li, Z. *Chem. Mater.* **2015**, *27*, 1847−1854.

(7) Zhao, Z. J.; Chen, S. M.; Lam, J. W. Y.; Lu, P.; Zhong, Y. C.; Wong, K. S.; Kwok, H. S.; Tang, B. Z. *Chem. Commun.* **2010**, *46*, 2221−2223.

(8) Thomas, K. R. J.; Velusamy, M.; Lin, J. T.; Tao, Y. T.; Chuen, C. H. *Adv. Funct. Mater.* **2004**, *14*, 387−392.

(9) (a) Förster, T.; Kasper, K. *Z. Phys. Chem.* **1954**, *1*, 275−277. (b) Birks, J. B., Ed. *Photophysics of Aromatic Molecules*; Wiley: London, 1970; pp 403−491.

(10) (a) Gierschner, J.; Park, S. Y. *J. Mater. Chem. C* **2013**, *1*, 5818−5832. (b) Huang, Y.-S.; Gierschner, J.; Schmidtke, J. P.; Friend, R. H.; Beljonne, D. *Phys. Rev. B: Condens. Matter Mater. Phys.* **2011**, *84*, No. 205311. (c) Gierschner, J.; Lüer, L.; Milián-Medina, B.; Oelkrug, D.; Egelhaaf, H.-J. *J. Phys. Chem. Lett.* **2013**, *4*, 2686−2697. (d) Chan, J. M. W.; Tischler, J. R.; Kooi, S. E.; Bulovic, V.; Swager, T. M. *J. Am. Chem. Soc.* **2009**, *131*, 5659−5666. (e) An, B.-K.; Kwon, S.-K.; Jung, S.-D.; Park, S. Y. *J. Am. Chem. Soc.* **2002**, *124*, 14410−14415.

(11) (a) Hong, Y.; Lam, J. W. Y.; Tang, B. Z. *Chem. Commun.* **2009**, *45*, 4332−4353. (b) Hong, Y. N.; Lam, J. W. Y.; Tang, B. Z. *Chem. Soc. Rev.* **2011**, *40*, 5361−5388.

(12) (a) Mei, J.; Leung, N. L. C.; Kwok, R. T. K.; Lam, J. W. Y.; Tang, B. Z. *Chem. Rev.* **2015**, *115*, 11718−11940. (b) Li, Z.; Dong, Y. Q.; Mi, B. X.; Tang, Y. H.; Haüssler, M.; Tong, H.; Dong, Y. P.; Lam, J. W. Y.; Ren, Y.; Sung, H. H. Y.; Wong, K. S.; Gao, P.; Williams, I. D.; Kwok, H. S.; Tang, B. Z. *J. Phys. Chem. B* **2005**, *109*, 10061−10066. (c) Shen, X. Y.; Wang, Y. J.; Zhao, E. G.; Yuan, W. Z.; Liu, Y.; Lu, P.; Qin, A. J.; Ma, Y. G.; Sun, J. Z.; Tang, B. Z. *J. Phys. Chem. C* **2013**, *117*, 7334−7347.

(13) (a) Tang, B. Z., Qin, A., Ed. *Aggregation-Induced Emission: Fundamentals*; Wiley, 2013; pp 323−335. (b) Yoshii, R.; Hirose, A.; Tanaka, K.; Chujo, Y. *J. Am. Chem. Soc.* **2014**, *136*, 18131−18139. (c) Ito, S.; Hirose, A.; Yamaguchi, M.; Tanaka, K.; Chujo, Y. *J. Mater. Chem. C* **2016**, *4*, 5564−5571. (d) Qian, L.; Tong, B.; Shen, J.; Shi, J.; Zhi, J.; Dong, Y.; Yang, F.; Dong, Y.; Lam, J. W. Y.; Liu, Y.; Tang, B. Z. *J. Phys. Chem. B* **2009**, *113*, 9098−9103. (e) Garg, K.; Ganapathi, E.; Rajakannu, P.; Ravikanth, M. *Phys. Chem. Chem. Phys.* **2015**, *17*, 19465−19473. (f) Chen, Z.; Zhang, J.; Song, M.; Yin, J.; Yu, G.-A.; Liu, S. H. *Chem. Commun.* **2015**, *51*, 326−329. (g) Naito, H.; Morisaki, Y.; Chujo, Y. *Angew. Chem., Int. Ed.* **2015**, *54*, 5084−5087.

(14) (a) Chandrasekaran, Y.; Venkatramaiah, N.; Patil, S. *Chem. − Eur. J.* **2016**, *22*, 5288−5294. (b) He, J. T.; Xu, B.; Chen, F. P.; Xia, H. J.; Li, K. P.; Ye, L.; Tian, W. J. *J. Phys. Chem. C* **2009**, *113*, 9892−9899. (c) Dong, Y. J.; Xu, B.; Zhang, J. B.; Lu, H. G.; Wen, S. P.; Chen, F. P.; He, J. T.; Li, B.; Ye, L.; Tian, W. J. *CrystEngComm* **2012**, *14*, 6593−6598. (d) Huang, J.; Sun, N.; Yang, J.; Tang, R.; Li, Q.; Ma, D.; Qin, J.; Li, Z. *J. Mater. Chem.* **2012**, *22*, 12001−12007.

(15) Wu, Q.; Zhang, T.; Peng, Q.; Wong, D.; Shuai, Z. *Phys. Chem. Chem. Phys.* **2014**, *16*, 5545−5552.

(16) Laughlin, R. G. *J. Am. Chem. Soc.* **1967**, *89*, 4268−4271.

DOI: 10.1021/acsomega.6b00335
ACS Omega 2016, 1, 1336−1342

(17) Zhou, X.; He, J.; Liao, L. S.; Lu, M.; Ding, X. M.; Hou, X. Y.; Zhang, X. M.; He, X. Q.; Lee, S. T. *Adv. Mater.* **2000**, *12*, 265−269.
(18) Li, Z. R., Ed. *Organic Light-emitting Materials and Devices*, 2nd ed.; CRC Press: Boca Raton, 2015; pp 60−62.
(19) Katoh, R.; Suzuki, K.; Furube, A.; Kotani, M.; Tokumaru, K. *J. Phys. Chem. C* **2009**, *113*, 2961−2965.
(20) (a) Chen, W.-C.; Wu, G.-F.; Yuan, Y.; Wei, H.-X.; Wong, F.-L.; Tong, Q.-X.; Lee, C.-S. *RSC Adv.* **2015**, *5*, 18067−18074. (b) Park, Y.; Kim, S.; Lee, J.-H.; Jung, D. H.; Wu, C.-C.; Park, J. *Org. Electron.* **2010**, *11*, 864−871.
(21) (a) Liu, H.; Bai, Q.; Yao, L.; Zhang, H.; Xu, H.; Zhang, S.; Li, W.; Gao, Y.; Li, J.; Lu, P.; Wang, H.; Yang, B.; Ma, Y. *Chem. Sci.* **2015**, *6*, 3797−3804. (b) Liu, Z.; Wu, S.; Bai, Y.; Jiang, W.; Hong, L.; Lei, T.; Ge, Z. *RSC Adv.* **2016**, *6*, 70008−70011.

DOI: 10.1021/acsomega.6b00335
ACS Omega 2016, 1, 1336−1342